Ground and Low-Lying Excited States of Phenoxy, 1-Naphthoxy and 2-Naphthoxy Radicals via Anion Photoelectron Spectroscopy

Steven J. Kregel and Etienne Garand*

Department of Chemistry, University of Wisconsin-Madison, 1101 University Ave., Madison, WI, USA.

*Corresponding Author: egarand@wisc.edu

Abstract

We present the slow electron velocity map imaging spectroscopy of cryogenically cooled phenoxide, 1-naphthoxide and 2-naphthoxide anions. The results allow us to examine the ground state and the lowest energy excited state in the corresponding neutral radicals. Care was taken to minimize autodetachment signals in the photoelectron spectra, allowing for more straightforward comparisons with Franck-Condon analyses. The ground states of these three aromatic oxide radicals all have the unpaired electron residing in an π orbital delocalized throughout the molecule. The electron affinity of 1-naphthoxy is measured to be 2.290(2) eV, while that of 2-naphthoxy is measured to be 2.404(2) eV, both of which are higher than that of the smaller phenoxy molecule at 2.253(1) eV. The first excited states have the unpaired electron residing in a more localized σ orbital, yielding measured term energies for the $\tilde{A}$ state of 1.237(2) eV in 1-naphthoxy and 1.068(1) eV in 2-naphthoxy, while that of phenoxy is lower at 0.952(1) eV. The calculated Franck-Condon spectra generally showed good agreement with the experimental spectra, yielding assignments of the more active vibrations in each electronic state. Significant autodetachment signals arising from dipole bound states near the ground states of all three radicals were observed in our efforts to avoid them, and comparably less autodetachment signals were observed near the excited states. Besides this type of non-Franck-Condon intensities in the photoelectron spectra, we also observed minor features arising due to vibronic coupling in the ground states of all three radicals.

I. Introduction

Aromatic oxide free radicals play an important role in atmospheric,[1] combustion,[2] and interstellar[3] chemistry. The nominal lone pairs on the oxygen atom can readily mix with the aromatic system, giving rise to close-lying electronic states that exhibit different extents of electron delocalization, which can in turn influence molecular reactivity. The presence of the oxide also imparts a significant dipole moment to the otherwise non-polar aromatic system, where the oxygen often serves in an electron-withdrawing role. These large dipole moments can lead to interesting electronic behaviors such as the presence of dipole-bound and resonance states.[4-6] The simplest of these aromatic oxide radicals is phenoxy, which has been shown to be a key intermediate in gasoline combustion and contributor to ozone and secondary organic aerosol production.[2] The larger naphthoxy radicals have been shown to undergo self-reactions to produce secondary organic aerosols,[1] and 2-naphthoxy is also believed to play an important role in excited state proton transfer which gives rise to dual fluorescence in 2-naphthol.[7] In this paper, we present the high resolution photoelectron (PE) spectroscopy of the phenoxide, 1-naphthoxide, and 2-naphthoxide anions, allowing us to study the energetics and vibrations of the ground and first excited states of the neutral aromatic oxide radicals.

There is a plethora of experimental and theoretical studies on the phenoxy radical. It has C_{2v} symmetry in its ground $\tilde{X}\,^2B_1$ state and low-lying excited $\tilde{A}\,^2B_2$ state, and the one-photon $\tilde{A} \leftarrow \tilde{X}$ transition is nominally symmetry forbidden. The vibrational frequencies of the phenoxy ground state have been measured in rare-gas matrices by infrared absorption,[8] in solution by resonance Raman,[9, 10] and in the gas phase by anion PE spectroscopy.[11, 12] The electronic transitions of phenoxy have been studied by UV-Vis absorption in the gas phase[13] and in rare-gas matrices,[14] and rovibronic bands of the $\tilde{A} \leftarrow \tilde{X}$ transition were detected via cavity-ringdown spectroscopy.[15] The origin of the $\tilde{A}$ state was first tentatively reported at 8550 cm^{-1} above the ground state in a PE spectroscopy study by Gunion *et al.*[11], but was later refined to 7681 cm^{-1} in the cavity ringdown study,[15] which attributed the larger value from

the PE spectrum to an unresolved band consisted of ν_{12} and ν_{17} modes. Finally, the ~4 Debye dipole moment of phenoxy is sufficiently large to support dipole bound states (DBS), in which an electron is loosely attached to the neutral molecule by long range forces.[4-6] Liu *et al.*[4] utilized high resolution PE spectroscopy to investigate these DBS in phenoxy and showed that the loosely bound electron has little effect on the structure of the neutral core, but autodetachment via DBS yielded greatly varying intensities in the resulting PE spectrum. This allowed for observation and assignment of vibrational modes that are absent in direct photodetachment spectrum.[5]

Compared to phenoxy, the larger 1-naphthoxy and 2-naphthoxy radicals, isomers differing in the location of the oxygen atom on the naphthyl ring, have undergone fewer spectroscopic investigations. The infrared spectrum of 2-naphthoxy was first reported by Sekine *et. al.*[7] who produced the radical through UV photolysis in an argon matrix. Additionally, electron spin resonance spectra of both 1-naphthoxy and 2-naphthoxy radicals were acquired by Dixon *et al.*[16] to yield the proton coupling constants. To the best of our knowledge, there has been no previous PE spectroscopy study on the naphthoxy radicals.

Here, we present the PE spectra of cryogenically-cooled phenoxide, 1-naphthoxide, and 2-naphthoxide anions, acquired using the higher-resolution slow electron velocity map imaging (SEVI)[17] approach. Utilizing a wide range of photon energies, we measured the electron affinities (EA) and the first excited state term energies for all three radicals. Moreover, we took care to avoid PE signal related to autodetachment processes, allowing us to assign the vibrational features with the aid of Franck-Condon calculations. Further analyses and comparisons of the three systems shed light on how the size of the aromatic system and position of the oxygen atom influence the electronic structures of these radicals.

II. Experimental and Theoretical Details

SEVI images were acquired using a homebuilt anion SEVI spectrometer described in detail previously.[18] It has been adapted with an electrospray ionization (ESI) source for the current set of experiments. Briefly, phenoxide, 1-naphthoxide or 2-naphthoxide anions were produced via ESI of a ~1 mM phenol, 1-naphthol, or 2-naphthol in methanol solution made slightly basic with trace amounts of KOH. The alkoxide anions were guided via ion guides through three differentially pumped stages into a 3D quadrupole ion trap held at 10 K, where they were thermalized via collisions with buffer gas consisted of 10% D_2 in helium. The cooled anions were ejected from the ion trap into a Wiley-McLaren time-of-flight mass spectrometer for mass separation. The anions of interest were selected via pulsed re-referencing prior to entering the multiplate velocity map imaging (VMI) region, where they were intersected with the output of a tunable 10 Hz optical parametric oscillator (OPO) laser. The resulting photoelectrons were imaged with a pair of 40 mm microchannel plates (MCPs) coupled to a phosphor screen, monitored by a 2048 x 2048 pixels CMOS camera. The SEVI images were acquired with the VMI repeller set at -500 V, and 50k-100k laser shots were summed for each image. To obtain the PE spectrum, each SEVI image was circularized,[19] quadrant symmetrized, inverse Abel transformed[20] and radially integrated. Calibrations of radial position to electron kinetic energy (eKE) were carried out using the $^2P_{3/2} \leftarrow {}^1S_0$ photodetachment transition of atomic iodide. For easier comparisons of PE spectra acquired with different photon energies, the spectra are presented as a function of electron binding energy (eBE), which is the difference between the photon energy and the measured eKE. The reported peak positions and uncertainties correspond to the fitted gaussian centers and half widths at half maximum. The anisotropy of spectral features was determined by fitting the angular intensity distribution of the most intense part of a feature to the equation $I(\theta) = \frac{\sigma}{4\pi}\left(1 + \beta P_2(cos\theta)\right)$, with P_2 being the second order Lagrange polynomial. Note that β values are expected to vary as a function of eKE due to Wigner's threshold law,[21] and weak or partially resolved features are expected to yield greater uncertainties in their fitted β values.

To facilitate comparisons with calculations, SEVI images were acquired at photon energies that minimized autodetachment signals related to excitations to DBS, which all three species studied here can support. To figure out which photon energies were suitable, we roughly mapped out the DBS transitions by monitoring the total photoelectron yield within the SEVI image while scanning the photon energy in 3 cm^{-1} increments (each data point was averaged for 500 laser shots). These spectra are shown in Figure S8 in supplementary material, and noticeably, transitions to DBS appear as dramatic enhancements in the photoelectron yield.

To aid the analyses of the experimental SEVI spectra, geometry optimization and harmonic frequency calculations were carried out at the cam-B3LYP/aug-cc-PVTZ level using the Gaussian 09[22] software package. Excited state calculations were performed using time-dependent density function theory (TDDFT) at the same level. The calculated vibrational frequencies are scaled by 0.974, determined by comparison to the previously reported vibrational frequencies of phenoxy.[8] Franck-Condon (FC) simulations accounting for the Duschinsky rotation effect were carried out using ezSpectrum[23] using the optimized geometries, vibrational displacements and scaled frequencies of the cam-B3LYP/aug-cc-PVTZ calculations. The FC spectra are aligned to the SEVI spectra at the origin transition for each electronic state.

III. Results and Assignments

a. Phenoxide anion

The closed-shell phenoxide anion has a calculated electron configuration of $\ldots\pi(b_1)^2\pi(a_2)^2\sigma(b_2)^2\pi(b_1)^2$. Removing one of the electrons from the HOMO, shown in Figure 1, results in the $\tilde{X}\,^2B_1$ ground state of the phenoxy radical. This π orbital has electron density well delocalized throughout the molecule, with the oxygen $2p_x$ orbital conjugated into the aromatic π system. The SEVI spectra corresponding to this transition are shown in Figure 1A; wider spectral range and additional

spectra are included in supplementary material. The nominally allowed vibrational modes in PE spectroscopy are those that are totally symmetric, which for phenoxy would be progressions of a_1 vibrations or overtone/combination modes of non-a_1 vibrations. The transition strengths of these modes can be estimated using the FC approximation, and the calculated FC spectrum is shown in Figure 1B. Overall, the FC spectrum shows good agreement with the SEVI spectra, allowing for assignment of most of the observed features, detailed in Table 1.

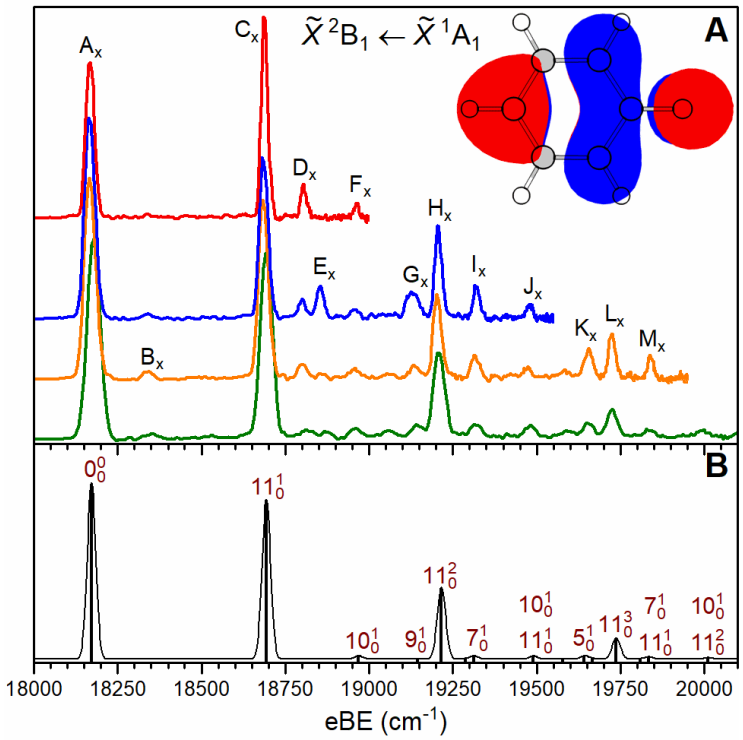

Figure 1. (A) SEVI spectra of the phenoxide anion acquired with photon energies of 18998 cm^{-1} (red), 19548 cm^{-1} (blue), 19949 cm^{-1} (orange) and 21000 cm^{-1} (green). Insert shows the HOMO of the anion ground state. (B) FC simulation of the $\tilde{X}\,^2B_1 \leftarrow \tilde{X}\,^1A_1$ transition.

Peak A_X is assigned to the origin transition, yielding a measured EA of 18172(9) cm^{-1} (2.253(1) eV), in excellent agreement with previous experiments.[4, 12] The calculated value of 17556 cm^{-1} shows an underestimation of the EA, and the open-shell neutral molecule, exhibiting slight spin contamination (S^2 = 0.81), is likely the major source of errors. The most FC active modes on the ground state involve the a_1 symmetry ν_{11} vibration with in-plane benzyl CCC bending motions, giving rise to the more intense peaks C_x, H_x and L_x, similar to what was observed by Kim *et al.*[12] Peaks F_x, G_x, I_x-K_x, and M_x are weaker features that were not observed previously by Kim *et al.*, but show good agreement to the FC simulation. Their assignments and peak positions are listed in Table 1, and the observed frequencies generally agree well with previously measured values.

Peaks B_X, D_X, and E_X are not accounted for by the FC analysis. The weak peak B_X at eBE = 18340(17) cm^{-1} (+168 cm^{-1}) must be the 20_0^1 transition because there are no other vibrations with frequencies this low. The ν_{20} vibration has a b_1 symmetry with out-of-plane CO bending motions. While the frequency of this vibration has not been previously reported in gas or condensed phase, the position of peak B_x agrees reasonably well with the calculated frequency of 185 cm^{-1}, providing good support for this assignment. Peak D_X at +633 cm^{-1} is assigned to another b_1 vibration, ν_{18}, which has out-of-plane CH bending motions. The observed frequency is in excellent agreement with previous measurements.[4, 8] This 18_0^1 transition was observed in a previous PE experiment,[4] and its presence was attributed to vibronic coupling. Similarly, we attribute the presence of peaks B_X and D_X here to vibronic coupling due to their fairly consistent intensities in SEVI spectra acquired at various photon energies. Peak E_X at +682 cm^{-1} is assigned to the $11_0^1 20_0^1$ transition based on the fundamental frequencies, which indicate this combination mode should occur at 684 cm^{-1}.

Table 1. Frequencies and assignments of the phenoxy radical. All values are in cm^{-1}. β values are determined using SEVI images acquired at 19949 cm^{-1} and 28890 cm^{-1}.

	eBE	Exp. Freq.	Calc. Freq.	β	Assignment	Previous Exp. Freq.
			$\tilde{X}\,^2B_1 \leftarrow \tilde{X}\,^1A_1$			
A_X	18172(9)	0	17556	-0.4	0_0^0	18173[a]
B_X	18340(17)	168	185	0.2	$20_0^1(b_1)$	
C_X	18688(12)	516	522	-0.4	$11_0^1(a_1)$	520[b]
D_X	18804(11)	633	643	0.1	$18_0^1(b_1)$	635[b]
E_X	18853(13)	682	707	0.1	$11_0^1 20_0^1$	
F_X	18963(9)	791	796	0	$10_0^1(a_1)$	790[a]
G_X	19136(22)	965	973	0	$9_0^1(a_1)$	977[b]
H_X	19206(12)	1034	1044	-0.3	11_0^2	1038[c]
I_X	19320(11)	1149	1141	0	$7_0^1(a_1)$	1167[b]
J_X	19478(10)	1307	1318	0	$10_0^1 11_0^1$	
K_X	19654(16)	1483	1470	0	$5_0^1(a_1)$	1481[b]
L_X	19724(12)	1552	1566	-0.2	11_0^3	1534[c]
M_X	19840(10)	1668	1663	0.1	$7_0^1 11_0^1$	
			$\tilde{A}\,^2B_2 \leftarrow \tilde{X}\,^1A_1$			
A_A	25849(11)	0	26263	0.1	0_0^0	25853[d]
B_A	26366(7)	517	518	0	$11_0^1(a_1)$	
C_A	26663(20)	814	823	0.1	$10_0^1(a_1)$	
D_A	26824(19)	975	990	0.3	$9_0^1(a_1)$	
E_A	26880(17)	1030	1036	0.2	11_0^2	
F_A	27084(16)	1235	1247	0	$6_0^1(a_1)$	
G_A	27179(20)	1330	1323	0.1	$25_0^1(b_2)$	
H_A	27436(17)	1586	1594 1624	0.3	$23_0^1(b_2)$ $4_0^1(a_1)$	
I_A	27598(16)	1749	1765	0	$6_0^1 11_0^1$	

[a] Ref. 4
[b] Ref. 8
[c] Ref. 12
[d] Ref. 15

Moreover, there are no other vibrations with a calculated frequency near this value. Similarly, peak I_x may very well be overlapped with the $11_0^1 18_0^1$ combination mode. Note that the intensity of peak E_X is significantly enhanced only in the image acquired with photon energy of 19548 cm^{-1}. Hence, we suspect that the 19548 cm^{-1} spectrum has some DBS related intensity enhancements.

Removing one of the electrons from the σ(b_2) HOMO-1, shown in Figure 2, results in the low-lying $\tilde{A}\ ^2B_2$ excited state of the phenoxy radical. This orbital has the oxygen $2p_y$ orbital conjugating into the benzyl σ system, but the electron density is mostly localized near the C-O bond. The SEVI spectra corresponding to this transition are shown in Figure 2A, and the calculated FC spectrum is shown in Figure 2B. The overall agreement between calculated and experimental spectra allows for assignment of most of the observed features, detailed in Table 1.

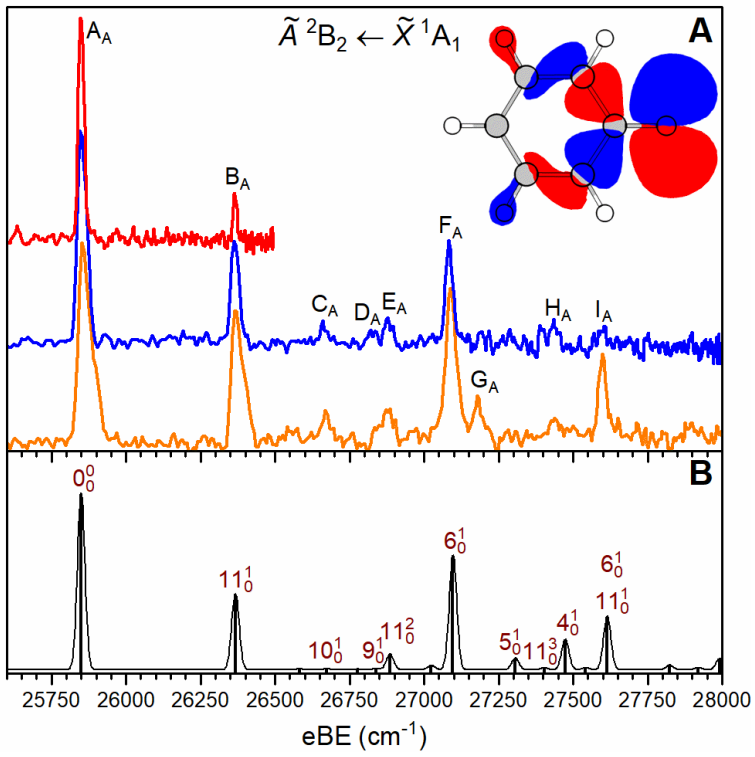

Figure 2. (A) SEVI spectra of the phenoxide anion acquired with photon energies of 26494 cm^{-1} (red), 27992 cm^{-1} (blue) and 28890 cm^{-1} (orange). Insert shows the HOMO-1 of the anion ground state. (B) FC simulation of the $\tilde{A}\ ^2B_2 \leftarrow \tilde{X}\ ^1A_1$ transition.

Peak A_A is assigned to the origin transition and it is a more dominant feature in the SEVI spectra compared to the ground state A_X peak. Its position at eBE = 25849(11) cm^{-1} gives a term energy of 7678(11) cm^{-1} (0.952(1) eV) for the $\tilde{A}\ ^2B_2$ state, which shows an excellent agreement with the 7681 cm^{-1} value determined by the cavity ringdown experiment.[15] The calculated value of 26263 cm^{-1} for the $\tilde{A}\ ^2B_2$

← $\tilde{X}\,^1A_1$ transition shows an overestimation, and again, the errors are likely related to the open-shell nature of the neutral species. Similar to the neutral ground state, modes involving the a_1 ν_{11} vibration are FC active, and the observed ν_{11} frequency of 517 cm^{-1} is essentially the same as that in the $\tilde{X}\,^2B_1$ state. In addition, modes involving the a_1 ν_6 vibration show significant FC activities on the $\tilde{A}$ state. This is a C-O stretching vibration, and the observed frequency at 1235 cm^{-1} is redshifted by ~250 cm^{-1} compared to the similar C-O stretching vibration (ν_5) on the $\tilde{X}$ state. Assignments of weaker features based on the FC analysis yielded frequencies of 814 cm^{-1} for ν_{10} and 975 cm^{-1} for ν_9 CCC bending vibrations, both of which have similar frequencies in the $\tilde{X}$ state.

The only obvious feature not captured by FC simulation is peak G_A, which is most intense in the spectrum acquired with photon energy of 28990 cm^{-1}. Based on its frequency at eBE = 27179(20) cm^{-1} (+1330 cm^{-1}), we assign it to the 25_0^1 transition. ν_{25} is an in-plane CH bend vibration with b_2 symmetry with a calculated frequency of 1323 cm^{-1}. In addition to gaining intensities via DBS, it may also gain some of its observed intensity via similar vibronic coupling mechanism that provided intensity for the b_1 modes on the $\tilde{X}$ state.[4, 24] Note that peak H_A, observed at +1586 cm^{-1}, can be alternatively assigned to either 23_0^1 or 4_0^1 transition, with the former having a better agreement with calculated frequency. The in-plane CC stretch ν_{23} vibration also has a b_2 symmetry, and it may very well be overlapped with the FC allowed 4_0^1 transition.

b. 1-Naphthoxide anion

The $\tilde{X}\,^2A''$ state of neutral 1-naphthoxy has a calculated dipole moment of 4.0 Debye, on par with phenoxy. Hence, we expect that it can also support DBS. Indeed, Figure S8 shows that photodetachment from the 1-naphthoxide anion accesses numerous DBS, and it is not trivial finding photon energies that would yield minimal autodetachment signals, especially at energies >19000 cm^{-1}. While SEVI spectra showing contributions arising from the DBS are interesting on their own,[4, 5] they do

make spectral assignment more difficult due to poor agreements with FC calculations, see Figure S4 for an example. For a lower symmetry molecule with more vibrations than phenoxy, assignments based solely on calculated frequencies without input from FC analyses is likely to be less reliable. Hence, in this paper we will focus mainly on the SEVI spectra showing minimal contributions from autodetachment.

The 1-naphthoxide anion has a calculated electron configuration of $\ldots\pi(a'')^2\pi(a'')^2\sigma(a')^2\pi(a'')^2$. Removing one of the electrons from the HOMO, shown in Figure 3, results in the $\tilde{X}\,^2A''$ ground state of the 1-naphthoxy radical. This π orbital is delocalized throughout the molecule, but most of the electron density is on the ring containing the oxygen atom, making it closely resembling the HOMO of phenoxide. The SEVI spectra corresponding to this $\tilde{X}\,^2A'' \leftarrow \tilde{X}\,^1A'$ transition are shown in Figure 3A. The calculated FC spectrum in Figure 3B shows a good agreement with the SEVI spectra, allowing us to assign the major features. Unfortunately, the density of FC modes and their overlapping frequencies in the eBE >19250 cm^{-1} region make assignment of the minor SEVI features quite difficult. The calculated vibrational frequencies are included in supplementary material for further considerations.

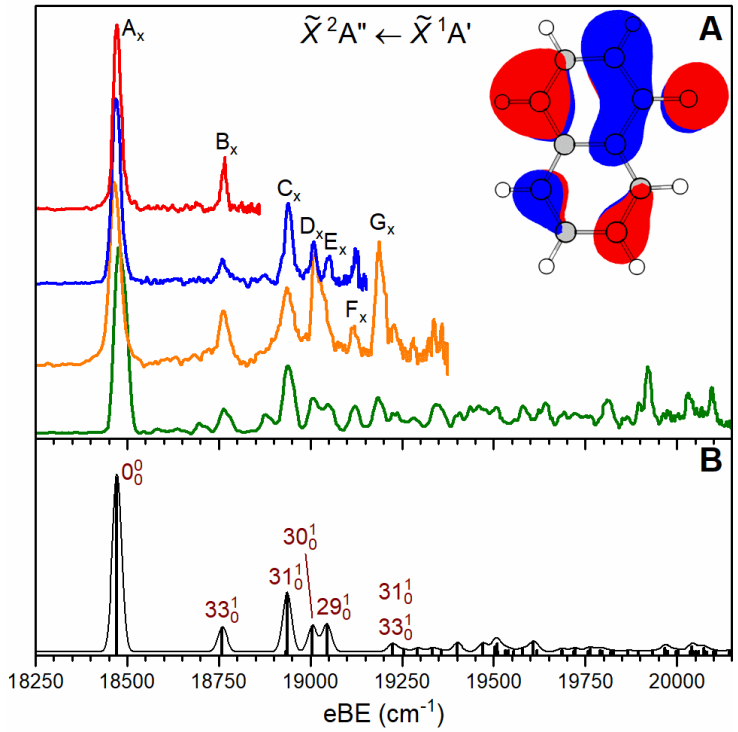

Figure 3. (A) SEVI spectra of the 1-naphthoxide anion acquired with photon energies of 18861 cm-1 (red), 19152 cm-1 (blue), 19374 cm^{-1} (orange) and 20277 cm^{-1} (green). Insert shows the HOMO of the anion ground state. b) FC simulation of the $\tilde{X}\,^2A'' \leftarrow \tilde{X}\,^1A'$ transition.

Peak A_X is the most intense feature, and is assigned to the origin transition, yielding an EA of 18472(13) cm^{-1} (2.290(2) eV) for the 1-naphthoxy radical. Based on the FC analysis, peaks B_x, C_x, D_x, and E_x are assigned to the 33_0^1, 31_0^1, 30_0^1, and 29_0^1 transitions, respectively. These are all a' vibrations, where ν_{29} and ν_{31} have similar in-plane CCC bending motions as the most active ν_{11} mode in phenoxy. The calculated frequencies are all within 5 cm^{-1} of the experimental values; a summary of the peak assignments is presented in Table 2.

Table 2. Frequencies and assignments of the 1-naphthoxy radical. All values are in cm^{-1}. β values are determined using SEVI spectra acquired at 19152 cm^{-1} and 29994 cm^{-1}.

	eBE	Exp. Freq.	Calc. Freq.	β	Assignment
			X **^{2}A" ← $\tilde{X}$ ^{1}A'**		
A_X	18472(13)	0	17712	0	0_0^0
B_X	18764(9)	292	287	0.2	33_0^1(a')
C_X	18939(13)	467	464	0	31_0^1(a')
D_X	19008(10)	536	534	0	30_0^1(a')
E_X	19049(9)	577	573	0	29_0^1(a')
F_X	19124(13)	652	656	0	42_0^1(a'')
G_X	19189(14)	717	713 724		28_0^1(a') 41_0^1(a'')
			$\tilde{A}$ **^{2}A' ← $\tilde{X}$ ^{1}A'**		
A_A	28452(14)	0	29050	0	0_0^0
B_A	28929(12)	477	474	0.2	31_0^1(a')
C_A	29024(11)	572	569	0.2	29_0^1(a')
D_A	29487(17)	1035	1043	0.2	$29_0^1 31_0^1$
E_A	29675(14)	1224	1232	0.1	18_0^1(a')
F_A	29825(13)	1373	1376 1389	0	15_0^1(a') 14_0^1(a')
G_A	29968(10)	1516	1527	0	11_0^1(a')

Peaks F_X and G_X are absent in the FC spectrum, which shows no activity in the 19050-19220 cm^{-1} region; the blue shoulder on peak G_X agrees well with the FC predicted $31_0^1 33_0^1$ combination mode. Peak F_X, at +652 cm^{-1}, matches well with the 656 cm^{-1} calculated frequency of ν_{42}, and therefore is assigned to the 42_0^1 transition. This is an a" vibration with out-of-plane CH bending motions, and likely gains intensity via vibronic coupling given its consistent intensities in various SEVI spectra. Peak G_X, at +717 cm^{-1}, can be assigned to either the a' ν_{28} in-plane CCC bend vibration calculated at 713 cm^{-1} or the a" ν_{41} out-of-plane CH bend vibration calculated at 724 cm^{-1}. Although the majority of peak G_X intensity in the 19374 cm^{-1} spectrum is enhanced via DBS autodetachment, just as the intensity of peak D_X is enhanced in this image, peak G_X does appear in spectra acquired at other photon energies, also see additional spectra in Figure S4. Therefore, it is likely that sources other than autodetachment also contribute to the observed intensity of peak G_X.

Removing one of the electrons from σ(a′) HOMO-1, shown in Figure 4, results in the $\tilde{A}\,^2A'$ excited state of 1-naphthoxy. This orbital very closely resembles the σ(b_2) orbital in phenoxide shown in Figure 2. The SEVI spectra corresponding to this $\tilde{A}\,^2A' \leftarrow \tilde{X}\,^1A'$ transition are shown in Figure 4A. The calculated FC spectrum, shown in Figure 4B, has excellent agreements with the SEVI spectra, capturing all the major observed features.

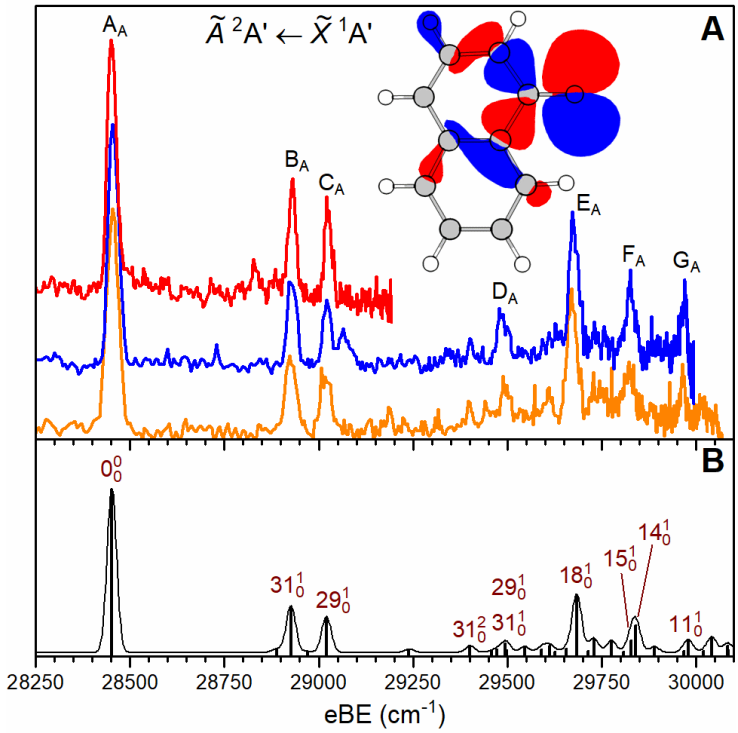

Figure 4. a) SEVI spectra of the 1-naphthoxide anion acquired with photon energies of 29193 cm^{-1} (red), 29994 cm^{-1} (blue) and 30100 cm^{-1} (orange). Insert shows the HOMO-1 of the anion ground state. b) FC simulation of the $\tilde{A}\,^2A' \leftarrow \tilde{X}\,^1A'$ transition.

Peak A_A, at eBE = 28452(14) cm^{-1}, is assigned to the origin transition, yielding a term energy for the $\tilde{A}$ state of 9980(14) cm^{-1} (1.237(2) eV). Peaks B_A at +477 cm^{-1} and C_A at +572 cm^{-1} are assigned to transitions to single quanta of v_{31} and v_{29} vibrations, respectively. These are the same CCC bending vibrations that are active in the $\tilde{X}$ state. Peak D_A is assigned to the combination mode $29_0^1 31_0^1$. Its experimental position at +1035 cm^{-1} matches well with the calculated 1043 cm^{-1} harmonic frequency, and although the combination mode overlaps with v_{24}, calculated at 1047 cm^{-1}, the FC simulation shows that the $29_0^1 31_0^1$ transition is more intense by a factor of four. Peak E_A, at +1224 cm^{-1}, is assigned to a vibration with significant FC activity, v_{18}. This is an in-plane a′ vibration with C-O stretching motion coupled with CH bend. Peak F_A, at +1373 cm^{-1}, is assigned to both 14_0^1 and 15_0^1 transitions based on the FC results, which indicate the v_{14} transition to be approximately twice as intense as v_{15}. These two vibrations are calculated to only differ in frequency by 13 cm^{-1} and are likely to be unresolved within peak F_A. Peak G_A

is assigned to the 11_0^1 transition, which is the most intense FC feature near the experimental frequency. This is an in-plane CC stretch and CH bend vibration. Lastly, there is a blue shoulder on peak C_A at +615 cm^{-1}, which only appears in the SEVI spectrum acquired with photon energy of 29994 cm^{-1}. Therefore, this feature is likely related to autodetachment processes, which are generally less active near the $\tilde{A}$ state, but can certainly exist. There is no fundamental vibrational frequency that matches the position of this feature, hence we attribute it to a combination mode.

c. 2-Naphthoxide anion

The $\tilde{X}\,^2A''$ state of neutral 2-naphthoxy has a calculated dipole moment of 4.8 Debye, larger than both phenoxy and 1-naphthoxy. As such, we observed autodetachment signals related to transitions via DBS in this molecule as well, see Figures S6 and S8. Additionally, we observed another type of autodetachment signal in 2-naphthoxy, characterized by well-resolved spectral features having the same eKE in SEVI spectra acquired with different photon energies. Hence, these features appear to have varying eBE and may be attributed to internal vibrational relaxation occurring in the DBS prior to autodetachment (see Figure S6 for an example). Therefore, care was taken to verify the consistency of a peak's eBE

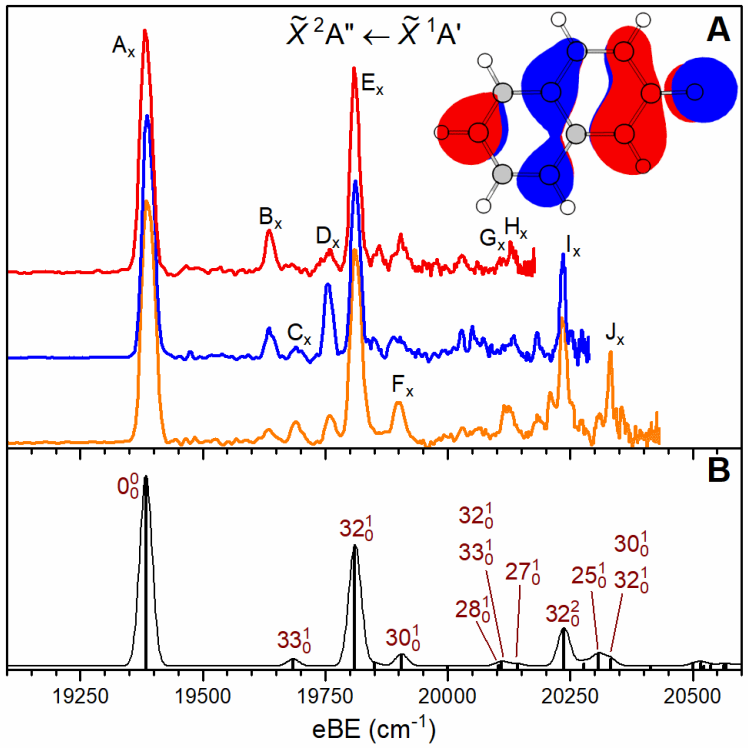

Figure 5. a) SEVI spectra of the 2-naphthoxide anion acquired with photon energies of 20177 cm^{-1} (red), 20288 cm^{-1} (blue) and 20432 cm^{-1} (orange). Insert shows the HOMO of the anion ground state. b) FC simulation of the $\tilde{X}\,^2A'' \leftarrow \tilde{X}\,^1A'$ transition.

position in at least two separate SEVI spectra before assignments were made.

The 2-naphthoxide anion has a calculated electron configuration of …$\pi(a'')^2\pi(a'')^2\sigma(a')^2\pi(a'')^2$. Removing one of the electrons from the HOMO, shown in Figure 5, results in the $\tilde{X}\,^2A''$ ground state of the 2-naphthnoxy radical. This π orbital again resembles the HOMO of phenoxide, differing from 1-naphthoxide mainly in the extent of delocalization to the adjacent benzyl ring due to difference in the oxygen position. The SEVI spectra corresponding to this $\tilde{X}\,^2A'' \leftarrow \tilde{X}\,^1A'$ transition are shown in Figure 5A, and the calculated FC spectrum is compared in Figure 5B.

Peak A_X is assigned to the origin transition, yielding an EA of 19388(14) cm^{-1} (2.404(2) eV) for 2-naphthoxy. The most intense modes excited in the $\tilde{X}\,^2A'' \leftarrow \tilde{X}\,^1A'$ transition involve the a' ν_{32} vibration, which is an in-plane CCC bending mode with most of the displacement localized to the oxygen containing benzyl ring. Hence, it is much the same vibration as the intense ν_{11} vibration in phenoxy. Transitions to the fundamental and overtone of ν_{32} give rise to peaks E_X and I_X. Peaks C_X and F_X are relatively weak features well reproduced by the FC calculation and are assigned to single excitations in the a' ν_{33} and ν_{30} vibrations, respectively. Peaks G_X and H_X are partially resolved from each other in the spectra acquired with photon energy of 20177 cm^{-1}. Based on the FC calculation, peak H_X is assigned to the 27_0^1 transition and peak G_X likely consists of

Table 3. Frequencies and assignments for the 2-naphthoxy radical. All values are in cm^{-1}. β values are determined using SEVI spectra acquired at 20432 cm^{-1} and 29958 cm^{-1}.

Peak	eBE	Exp. Freq.	Calc. Freq.	β	Assignment
			$\tilde{X}\,^2A'' \leftarrow \tilde{X}\,^1A'$		
A_X	19388(14)	0	18630	-0.6	0_0^0
B_X	19637(10)	248	258	0.3	46_0^1(a'')
C_X	19691(11)	303	300	0.1	33_0^1(a')
D_X	19756(9)	368	383	0.3	45_0^1(a'')
E_X	19810(11)	422	426	-0.4	32_0^1(a')
F_X	19900(15)	512	522	0.1	30_0^1(a')
G_X	20109(10)	721	720 726		28_0^1(a') $32_0^1 33_0^1$
H_X	20131(10)	743	758		27_0^1(a')
I_X	20235(6)	846	852	-0.1	32_0^2(a')
J_X	20332(10)	943	923 948		25_0^1(a') $30_0^1 32_0^1$
			$\tilde{A}\,^2A' \leftarrow \tilde{X}\,^1A'$		
A_A	28005(8)	0	28388	0	0_0^0
B_A	28413(10)	408	413	0.1	32_0^1(a')
C_A	28455(9)	450	456	0	31_0^1(a')
D_A	29189(25)	1183	1178 1207	0.1	20_0^1(a') 19_0^1(a')

two transitions, 28_0^1 and $32_0^1 33_0^1$, with the latter combination mode having almost six times stronger FC activity. Finally, peak J can be assigned to either 25_0^1 or $30_0^1 32_0^1$ transition.

Peaks B_X and D_X are notably absent in the FC simulation. Peak B_X, at +248 cm^{-1}, is assigned to the a'' ν_{46} vibration based on the agreement with the calculated frequency at 258 cm^{-1}. This is an out-of-plane ring deformation vibration with some out-of-plane CO bending motion. The fairly consistent intensity of peak B_X in the three spectra shown in Figure 5A indicates that ν_{46} likely gains intensity via vibronic coupling without significant mediation by DBS. Peak D_X, at +368 cm^{-1}, is assigned to the a'' ν_{45} vibration based on the calculated frequency of 383 cm^{-1}. This is also an out-of-plane ring deformation vibration. The ν_{45} vibration likely gains some of its intensity via vibronic coupling as it consistently shows up in all the SEVI spectra, although it appears to also pick up intensity via autodetachment processes as indicated by the 20288 cm^{-1} spectrum. Given the presence of these two non-FC modes, some of the minor features in the spectra may be combination modes involving these and FC allowed vibrations.

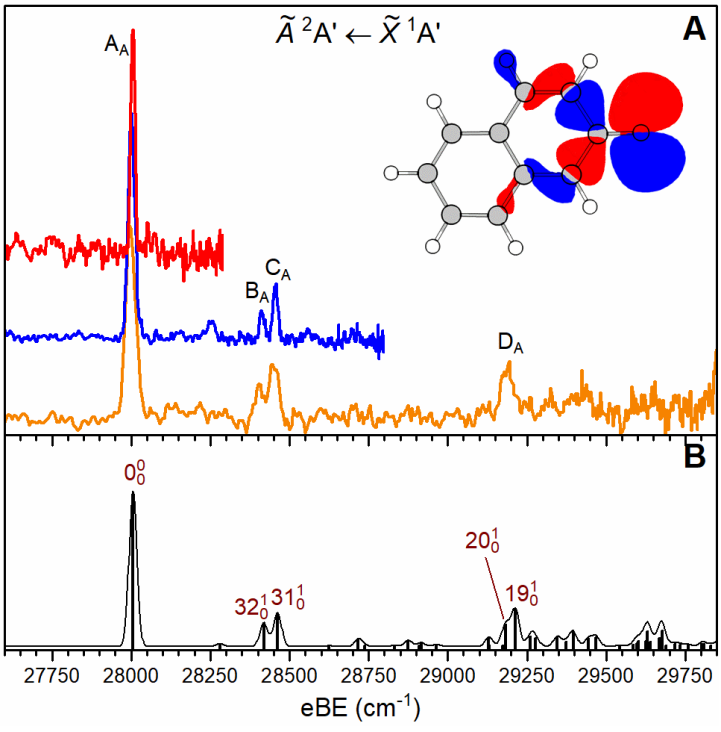

Figure 6. a) SEVI spectra of the 2-naphthoxide anion acquired with photon energies of 28288 cm^{-1} (red), 28796 cm^{-1} (blue) and 29958 cm^{-1} (orange). Insert shows the HOMO-1 of the anion ground state. b) FC simulation of the $\tilde{A}\,^2A' \leftarrow \tilde{X}\,^1A'$ transition.

Removing one of the electrons from σ(a') HOMO-1, shown in Figure 6, results in the $\tilde{A}\,^2A'$ excited state of 2-naphthoxy. The distribution of electron density in this orbital is very similar to the $\sigma(b_2)$ orbital in phenoxide. The SEVI spectra

corresponding to this $\tilde{A}\,^2A' \leftarrow \tilde{X}\,^1A'$ transition are shown in Figure 6A, and the calculated FC spectrum is shown in Figure 6B. Both the experimental and calculated spectra show relatively low intensities in the vibrational modes, yielding a dominant origin transition. Hence, peak A_A, assigned to the origin transition with a position of eBE = 28005(8) cm^{-1}, gives a term energy of 8617(14) cm^{-1} (1.068(2) eV) for the $\tilde{A}$ state. There are only three resolved vibrational features in the SEVI spectra, peaks B_A, C_A, and D_A. Peaks B_A and C_A are assigned to single excitation in the a' ν_{32} and ν_{31} vibrations, respectively. Both vibrations have in-plane CO and CCC bending displacements. Peak D_A likely contains two unresolved transitions, 19_0^1 and 20_0^1. Both a' vibrations involve in-plane CO stretching coupled with CH bending motions and are calculated to differ by only 29 cm^{-1}.

IV. Discussion

The molecular orbitals involved in our photodetachment studies of phenoxy, 1-naphthoxy and 2-naphthoxy show very similar electron distributions. Hence, the spectroscopic results of these three molecules share many similarities. The HOMO of the anions are π orbitals that have electron density well delocalized throughout the molecule. 1-naphthoxy and 2-naphthoxy, with larger π systems, have slightly larger EA (18472 cm^{-1} and 19388 cm^{-1}) than phenoxy (18172 cm^{-1}). However, while 1-naphthoxy shows a stabilization of 300 cm^{-1} in accommodating the excess electron, 2-naphthoxy shows a much greater stabilization of 1216 cm^{-1} relative to phenoxy. The term energies for the $\tilde{A}$ state are similarly larger for the molecules with a larger π system, but the exact trend between the three molecules differ than the $\tilde{X}$ state. Namely, the $\tilde{X} \rightarrow \tilde{A}$ energy is largest in 1-naphthoxy at 9980 cm^{-1}, followed by 2-naphthoxy at 8617 cm^{-1} and phenoxy at 7678 cm^{-1}. In the calculated results, the EA for all three molecules are calculated 600-800 cm^{-1} too low, while the eBE of the $\tilde{A}$ state are calculated 380-600 cm^{-1} too high. These errors are within typical DFT uncertainty,[25] but nonetheless seem to indicate systematic errors when calculating the electronic state involving singly-occupied π orbital vs. one involving singly-

occupied σ orbital. However, these errors appear to be relatively minor, and the optimized geometries and vibrational frequencies yielded FC spectra that generally show very good agreements with experimental SEVI spectra.

When accessing the $\tilde{X}$ state of the neutral radicals, an electron is ejected from the HOMO of the anion. In phenoxy, this π orbital has two parallel nodes perpendicular to the C-O bond, one along the CO bond itself and another in the middle of the benzyl ring. In 1-naphthoxy and 2-naphthoxy, the difference in the position of the extra benzyl ring relative to the C-O bond give rise to two different extension of electron density into the additional benzyl ring. Upon photodetachment to the neutral ground state, phenoxy shows dominant activity in ν_{11}, which is an a_1 mode with in-plane CCC bending motion that stretches the benzyl ring along the axis of the C-O bond. The associated geometry change shows two CCC angles expanding from 113.9° and 117.5° in the anion to 117.2° and 120.8° in the neutral radical. We note that these bond angles are in good agreement with previous calculations at the B3LYP/aug-cc-pVTZ level.[26] 2-naphthoxy shows dominant activity in essentially the same vibration, ν_{32}, with similar geometry changes (see supplementary material for details). 1-naphthoxy, on the other hand, does not have a single dominant active vibration. Rather, four vibrations show significant activity, where two of these, ν_{31} and ν_{29}, have CCC bending motions that are similar to ν_{11} in phenoxy. In addition to the changes in CCC angles, there is also a slight contraction in the CO bond length in all three molecules, from 1.256-1.263 Å in the anion to 1.232-1.244 Å in the neutral radical. This change is not surprising given that an electron is removed from an π orbital that has slight C-O antibonding characteristic, but it is not large enough to impart significant intensity to the CO stretch vibration in the SEVI spectrum.

In accessing the $\tilde{A}$ state of the neutral radicals, an electron is ejected from the HOMO-1 of the anion, which is an σ orbital involving the nominal 2p lone pair orbital on the oxygen atom that is perpendicular

to the benzyl π system. This σ molecular orbital is very similar in all three molecules. In phenoxy, the $\tilde{A}$ state shows changes in the CCC angles as well as a significant lengthening of C-O bond from 1.263 Å in the anion to 1.321 Å in the neutral. These geometry changes result in FC activity in the a_1 symmetry ν_{11} and ν_6 vibrations. The stronger ν_6 vibration is predominantly a C-O stretching vibration. Similarly, the FC active modes in 1-naphthoxy are the CCC bending vibrations ν_{31} and ν_{29} as well as CO stretch vibration ν_{18}. In 2-naphthoxy, there is a noticeable decrease in the overall FC vibrational activity in the $\tilde{A}$ state compared to the other two molecules, but the dominate vibrations are still the CCC bending ν_{32} and ν_{31} and CO stretching ν_{19} vibrations.

In addition to the FC allowed modes, we also observed minor activity in the non-totally symmetric vibrations that appear to gain intensity via vibronic coupling. These are out-of-plane vibrations ν_{20} and ν_{18} (b_1 symmetry) in the $\tilde{X}$ state and ν_{25} (b_2 symmetry) in the $\tilde{A}$ state of phenoxy, ν_{42} (a" symmetry) in the $\tilde{X}$ state of 1-naphthoxy, and ν_{46} and ν_{45} (a" symmetry) in the $\tilde{X}$ state of 2-naphthoxy. The $\tilde{X}$ state vibronically coupled modes of phenoxy, 1-naphthoxy and 2-naphthoxy appear with consistent intensities in multiple spectra. Moreover, those in phenoxy and 2-naphthoxy have a somewhat distinct anisotropy compared to nearby FC allowed modes. In contrast, vibronically coupled modes are less apparent in the $\tilde{A}$ state spectra, where they are absent in 1-naphthoxy and 2-naphthoxy, and in phenoxy, autodetachment processes may account for most of the observed intensity of the nominally forbidden transition.

Finally, the large dipole moments present in all three molecules give rise to significant autodetachment signals from excitations to the DBS, particularly in their $\tilde{X}$ state spectral regions. The SEVI spectra of the $\tilde{A}$ states also show evidence of autodetachment signals, albeit they are less pervasive. It is interesting to note that 2-naphthoxy, with the largest dipole moment, appears to have comparably longer-lived DBS that maybe undergoing vibrational relaxation prior to autodetachment. In the 2-naphthoxy SEVI spectra, such delayed autodetachment signals are distinguishable from prompt

detachment by their constant eKE in images acquired with different photon energies. Similar features have been observed previously in other systems,[27-30] and the dynamics of these prompt and delayed autodetachment processes are interesting on their own and may warrant additional detailed analyses of these spectra in the future.

V. Conclusion

SEVI spectroscopic study of the phenoxy, 1-naphthoxy and 2-naphthoxy radicals via their respective anions offer a close look at the ground and low-lying excited states of these aromatic oxide molecules. The EA and $\tilde{A}$ state term energies of phenoxy observed in our experiment are in excellent agreement with previous studies. The EA and $\tilde{A}$ state term energy of 1-naphthoxy and 2-naphthoxy are reported for the first time. Vibrational activities in the $\tilde{X}$ and $\tilde{A}$ state of 2-naphthoxy upon photodetachment from the anion ground state share greater similarities with phenoxy than 1-naphthoxy, which is likely related to the different positioning of the oxygen relative to the benzyl group. Overall, the three radicals share many similarities, including pervasive presence of DBS near the radical ground state, and the presence of vibronically coupled modes in the $\tilde{X} \leftarrow \tilde{X}$ transition.

Supplementary Material

See supplementary material for calculated geometries and vibrational frequencies, as well as additional SEVI spectra, images and energy dependent total photoelectron yields.

Acknowledgements

This work was supported by the U.S. Department of Energy, Office of Science, Basic Energy Sciences, under award No. DE-SC0010326. The computational resources used in this work are supported by National Science Foundation Grant CHE-0840494.

References

1. R. M. Healy, Y. Chen, I. Kourtchev, M. Kalberer, D. O'Shea and J. C. Wenger, Environ. Sci. Technol. **46**, 11813-11820 (2012).

2. J. Platz, O. J. Nielsen, T. J. Wallington, J. C. Ball, M. D. Hurley, A. M. Straccia, W. F. Schneider and J. Sehested, J. Phys. Chem. A **102**, 7964-7974 (1998).

3. M. Araki, Y. Matsushita and K. Tsukiyama, Astrophys. J. **150**, 113 (2015).

4. H. T. Liu, C. G. Ning, D. L. Huang, P. D. Dau and L. S. Wang, Angew. Chem. Int. Ed. **52**, 8976-8979 (2013).

5. D.-L. Huang, H.-T. Liu, C.-G. Ning and L.-S. Wang, J. Chem. Phys. **142**, 124309 (2015).

6. R. D. Mead, K. R. Lykke, W. C. Lineberger, J. Marks and J. I. Brauman, J. Chem. Phys. **81**, 4883-4892 (1984).

7. M. Sekine, H. Sekiya and M. Nakata, J. Phys. Chem. A **116**, 8980-8988 (2012).

8. J. Spanget-Larsen, M. Gil, A. Gorski, D. M. Blake, J. Waluk and J. G. Radziszewski, J. Am. Chem. Soc. **123**, 11253-11261 (2001).

9. A. Mukherjee, M. L. McGlashen and T. G. Spiro, J. Phys. Chem. **99**, 4912-4917 (1995).

10. G. N. R. Tripathi and R. H. Schuler, J. Chem. Phys. **81**, 113-121 (1984).

11. R. F. Gunion, M. K. Gilles, M. L. Polak and W. C. Lineberger, Int. J. Mass Spectrom. Ion Processes **117**, 601-620 (1992).

12. J. B. Kim, T. I. Yacovitch, C. Hock and D. M. Neumark, Phys. Chem. Chem. Phys. **13**, 17378-17383 (2011).

13. K. Tonokura, T. Ogura and M. Koshi, J. Phys. Chem. A **108**, 7801-7805 (2004).

14. J. G. Radziszewski, M. Gil, A. Gorski, J. Spanget-Larsen, J. Waluk and B. J. Mróz, J. Chem. Phys. **115**, 9733-9738 (2001).

15. C.-W. Cheng, H. Witek and Y.-P. Lee, J. Chem. Phys. **129**, 154307 (2008).

16. W. T. Dixon, W. E. J. Foster and D. Murphy, J. Chem. Soc., Perkin Trans. 2 **0**, 2124-2127 (1973).

17. D. M. Neumark, J. Phys. Chem. A **112**, 13287-13301 (2008).

18. S. J. Kregel, G. K. Thurston, J. Zhou and E. Garand, J. Chem. Phys. **147**, 094201 (2017).

19. J. R. Gascooke, S. T. Gibson and W. D. Lawrance, J. Chem. Phys. **147**, 013924 (2017).

20. E. W. Hansen and P.-L. Law, J. Opt. Soc. Am. A **2**, 510-520 (1985).

21. E. P. Wigner, Phys. Rev. **73**, 1002-1009 (1948).

22. Gaussian 09, Revision D.01, M. J. Frisch, G. W. Trucks, H. B. Schlegel, G. E. Scuseria, M. A. Robb, J. R. Cheeseman, G. Scalmani, V. Barone, B. Mennucci, G. A. Petersson, H. Nakatsuji, M. Caricato, X. Li, H. P. Hratchian, A. F. Izmaylov, J. Bloino, G. Zheng, J. L. Sonnenberg, M. Hada, M. Ehara, K. Toyota, R. Fukuda, J. Hasegawa, M. Ishida, T. Nakajima, Y. Honda, O. Kitao, H. Nakai, T. Vreven, J. A. Montgomery, J. E. Peralta, F. Ogliaro, M. Bearpark, J. J. Heyd, E. Brothers, K. N. Kudin, V. N. Staroverov, R. Kobayashi, J. Normand, K. Raghavachari, A. Rendell, J. C. Burant, S. S. Iyengar, J. Tomasi, M. Cossi, N. Rega, J. M. Millam, M. Klene, J. E. Knox, J. B. Cross, V. Bakken, C. Adamo, J. Jaramillo, R. Gomperts, R. E. Stratmann, O. Yazyev, A. J. Austin, R. Cammi, C. Pomelli, J. W. Ochterski, R. L. Martin, K. Morokuma, V. G. Zakrzewski, G. A. Voth, P. Salvador, J. J. Dannenberg, S. Dapprich, A. D. Daniels, O. Farkas, J. B. Foresman, J. V. Ortiz, J. Cioslowski and D. J. Fox, Gaussian, Inc., Wallingford CT, 2009

23. ezSpectrum, V. A. Mozhayskiy and A. I. Krylov, http://iopenshell.usc.edu/downloads

24. J. B. Kim, M. L. Weichman, T. I. Yacovitch, C. Shih and D. M. Neumark, J. Chem. Phys. **139**, 104301 (2013).

25. M. D. Wodrich, C. Corminboeuf, P. R. Schreiner, A. A. Fokin and P. v. R. Schleyer, Org. Lett. **9**, 1851-1854 (2007).

26. C. W. Cheng, Y. P. Lee and H. A. Witek, J. Phys. Chem. A **112**, 2648-2657 (2008).

27. Q.-q. Yuan, Z. Yang, R.-z. Li, W. J. Transue, Z.-p. Li, L. Jiang, N. Govind, C. C. Cummins and X.-B. Wang, Chin. J. Chem. Phys. DOI:10.1063/1674-0068/1031/cjcp1805114 (2018).

28. J. N. Bull and J. R. R. Verlet, Phys. Chem. Chem. Phys. **19**, 26589-26595 (2017).

29. J. N. Bull, C. W. West and J. R. R. Verlet, Phys. Chem. Chem. Phys. **17**, 16125-16135 (2015).

30. J. N. Bull, C. W. West and J. R. R. Verlet, Chemical Science **7**, 5352-5361 (2016).